PHYSICAL REVIEW B **84**, 115444 (2011)

Transport measurements on carbon nanotubes structurally characterized by electron diffraction

C. S. Allen,* M. D. Elkin, G. Burnell, and B. J. Hickey
School of Physics and Astronomy, University of Leeds, LS2 9JT, United Kingdom

C. Zhang, S. Hofmann, and J. Robertson
Department of Engineering, University of Cambridge, CB2 1PZ, United Kingdom

(Received 25 May 2011; published 23 September 2011)

A technique for the structural and electronic characterization of *the same* individual single wall carbon nanotube is presented. Electron diffraction was performed on carbon nanotubes grown across a perforated silicon nitride film and the chiral indices of individual tubes were determined. By means of a scanning-probe-based nanomanipulator a selected tube was then placed in the desired location across prepatterned electrodes. After patterning further electrodes on-top of the tube electronic transport measurements showed room temperature conductances of up to 0.2 G_0. The application of a gate voltage allowed the tuning of the room temperature conductance of the device and measurements at liquid helium temperatures showed signatures of a Coulomb blockade, indicating the formation of a carbon nanotube quantum dot.

DOI: 10.1103/PhysRevB.84.115444 PACS number(s): 81.05.ug, 81.16.−c, 61.05.J−

I. INTRODUCTION

Theoretical predictions of the sensitivity of the electronic properties of single-wall carbon nanotubes (SWCNTs) to their precise molecular structures have inspired much of the research into this fascinating material. Depending on the value of the chiral indices [denoted (n,m) where n and m are integers] SWCNTs fall into one of three categories: metallic, large band-gap semiconducting, or small band-gap semiconducting.[1,2]

To investigate these theoretical predictions an accurate and reliable method to determine the chiral indices of SWCNTs is needed. This challenge has been taken up by the optical spectroscopy,[3,4] electron microscopy,[5,6] and scanning probe[7] communities.

On their discovery, the chiral structure of SWCNTs was determined from the form of an electron diffraction pattern.[8] The analysis of electron diffraction patterns remains among the most accurate methods for the unambiguous determination of tube structure. However, recent advances in abberation corrected transmission electron microscopy[9] and in the understanding of optical signatures of SWCNTs[10] are making these increasingly powerful tools for the determination of the carbon nanotube structure.

In general, any growth of SWCNTs results in a variety of different chirality tubes, and to date it is not possible to grow specific structures *to order*, although there has been some success in narrowing the distribution of chiralities by careful control of growth conditions.[11] There have recently been great advances in techniques for postgrowth sorting SWCNTs from dispersion using surfactants[12] or DNA[13,14] which bind selectively to particular chirality tubes. Despite this, obtaining electronic transport measurements from SWCNTs of known chiral indices remains a challenge.

Attempts to combine structural characterization with electronic measurements on individual SWCNTs remain relatively few. The most notable examples being a print transfer technique combining optical spectroscopy and transport measurements,[15,16] electron diffraction with *in situ* transport measurements performed on double wall carbon nanotubes,[17] and electron diffraction or Raman spectroscopy on completed devices containing SWCNTs grown across slits in the substrate.[18,19]

In this work we determine the chiral indices of an individual SWCNT from the analysis of electron diffraction patterns. The chirality assigned tube is then manipulated to lie across palladium electrodes allowing electron transport measurements to be performed.

II. DEVICE FABRICATION

Carbon nanotubes were grown by chemical vapor deposition on a perforated silicon nitride transmission electron microscope (TEM) grid at 900 °C using a calcinated ferritin catalyst. This produces a low density of individual SWCNTs, double wall carbon nanotubes, and ropes containing a few tubes. The mean diameter of SWCNTs grown with this method is 2.7 nm with a standard deviation of 0.6 nm.

Real space images and electron diffraction patterns were obtained from tubes spanning holes in the substrate using a Philips/FEI CM200 TEM operating at 80 keV. An analysis of diffraction patterns from SWCNTs was performed and chiral indices determined.

The TEM grid was then transferred into a system consisting of four scanning tunneling microscope (STM) tips arranged in a cross geometry situated beneath a scanning electron microscope (SEM) all under an ultrahigh vacuum. Using the SEM for navigation, two opposing STM tips were brought into contact with the desired nanotube [Figs. 1(a) and 1(b)]. In general, the nanotube is broken at the point where it contacts the silicon nitride substrate with the portion spanning the hole remaining suspended between the STM tips. This limits the length of tube which can be lifted to $\sim 2\,\mu$m, the diameter of the perforations. Occasionally the tube is not broken at the edges of the hole and a longer length of tube can be peeled from the substrate.

Once the SWCNT was suspended, the tips were retracted vertically from the TEM grid and moved laterally apart until the tube became detached from one of the tips [Figs. 1(c) and 1(d)].

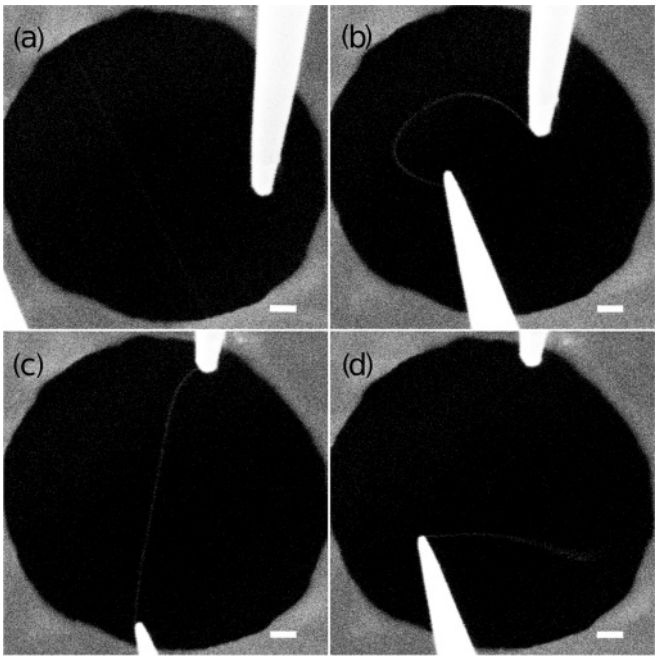

FIG. 1. SEM images showing picking of a SWCNT from the TEM grid with the tungsten STM tips (Ref. 20). The scale bars represent 200 nm.

The TEM grid was then removed and replaced with a substrate on which electrodes had be patterned by standard lithography techniques. A bias voltage of ∼2 V was applied between tip and electrode and, using the STM feedback electronics, the tube approached into tunneling contact. The tip was then retracted to the limits of the piezomotors and the STM electronics replaced with external source-sense electronics. With an applied bias voltage of 2 V the tube was approached toward the electrodes while the current flow was continually monitored. When the tube made physical contact with the electrode, current was seen to flow. Using the SEM for guidance, the tube was placed in the desired position across the electrodes (Fig. 2).

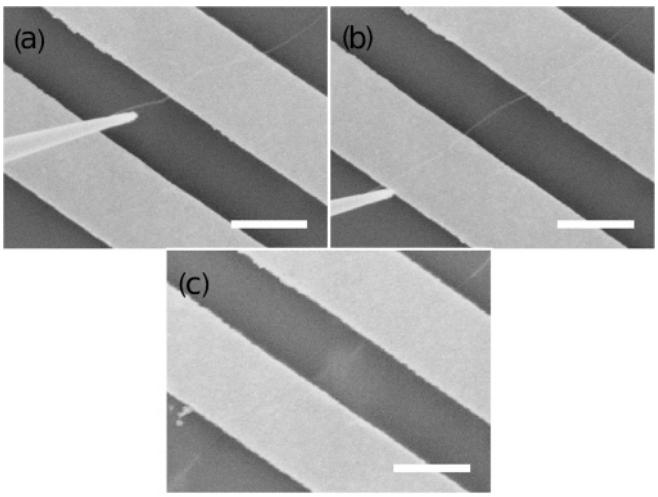

FIG. 2. SEM images showing placing of the carbon nanotube across prepatterned electrodes (Ref. 20). The scale bars represent 1 μm.

Using this technique we have successfully fabricated devices consisting of individual single and double-wall tubes as well as ropes containing multiple tubes.

III. RESULTS AND DISCUSSION

Figure 3 shows the diffraction pattern from an individual SWCNT. The pattern is made up of layer lines corresponding to reflections from the various planes of the graphene lattice elongated in the radial direction due to the curvature of the SWCNT.

To extract the chiral indices from the diffraction pattern we performed an analysis based on measurements of the axial positions of the layer lines[21–24] and their radial intensity distribution.[25–27] Measurements of the axial distance of each layer line from the equatorial line allow both the chiral angle[21] θ and the ratio of the chiral indices[22,23] n/m to be calculated. For the diffraction pattern shown in Fig. 3 we obtained values of $\theta = 25.8 \pm 0.2^\circ$ and $n/m = 0.773 \pm 0.005$. When combined with a diameter measurement from the real space image (Fig. 3 inset) of $D_0 = 2.6 \pm 0.5$ nm this suggests chiral indices of either (17,22) or (20,26). The large error in the diameter determined from the real space measurement is a consequence of experimental uncertainty and the difficulty in obtaining an accurate measurement due to the contribution of phase contrast to the image.[28]

The form of the radial intensity distribution of each of the layer lines is well described by the square of a Bessel function, the order of which is directly related to the chiral indices of the SWCNT.[25] By comparison of the measured radial intensity distribution with calculated squared Bessel functions, the chiral indices of the SWCNT can be determined.[26,27] When experimental uncertainties are taken into account this analysis suggests that the chiral indices lie in the range $15 \leqslant n \leqslant 18$ and $19 \leqslant m \leqslant 24$ with the sum of the chiral indices being $37 \leqslant n + m \leqslant 45$ and the difference $4 \leqslant m - n \leqslant 5$. Combining this analysis with the possible structures determined from the axial

FIG. 3. Electron diffraction pattern from an individual (17,22) SWCNT and real space image (insert, scale bar represents 5 nm).

measurements suggests a tube structure of (17,22). This tube structure can be confirmed by fitting the square of a Bessel function to the experimental data of each of the layer lines with only those corresponding to the correct chiral indices accurately describing the experimental data and giving a consistent value for the tube diameter.[29]

In this way the diffraction pattern shown in Fig. 3 was confidently determined to be from a (17,22) SWCNT.

The size of the band gap of a single-wall carbon nanotube can be estimated from the equation[30]

$$E_g = \frac{2a_0\gamma_0}{\sqrt{3}D_0}, \tag{1}$$

with a_0, the lattice constant of sp^2-bonded carbon (graphene), γ_0, the nearest-neighbor overlap integral, and D_0 the diameter of the tube. Taking $a_0 = 0.246$ nm (Ref. 31), $\gamma_0 = 2.9$ eV (Ref. 32), and the diameter of the SWCNT as 2.65 nm gives an estimated band gap of 0.31 eV. The extra contribution to the band gap due to curvature of the tube can be estimated using[33]

$$E_g^c = \frac{\gamma_0}{a_0^2} 4D_0^2 \cos 3\theta, \tag{2}$$

with θ the chiral angle of the SWCNT. For a (17,22) SWCNT, $\theta = 25.7^\circ$, giving $E_g^c = 0.0014$ eV an insignificant contribution to the total band gap.

Palladium electrodes were patterned using standard electron beam lithography (EBL) and sputter deposition techniques on a highly doped silicon substrate with a 200 nm silicon oxide cap. Using the technique described in Sec. II the individual (17,22) SWCNT was manipulated onto the Pd electrodes.

To improve the quality of the contacts a second set of Pd electrodes were patterned on top of the SWCNT using standard EBL and sputter deposition. The transport properties of the completed device are shown in Fig. 4. The room temperature I-V characteristics are linear with a conductance of 8.7 μS $\approx$ 0.2 G_0 where $G_0 = 38.7$ μS is the quantum of conductance.[34] The theoretical conductance through an individual SWCNT with perfectly transparent contacts to electrodes is $4G_0$ (Ref. 35).

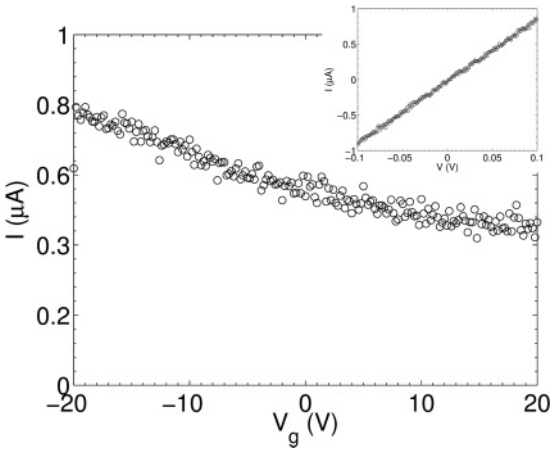

FIG. 4. Room temperature I-V characteristics (inset, measured at $V_g = 0$ V) and gate voltage response with $V_{sd} = 100$ mV of the individual (17,22) SWCNT device. I-V characteristics remain linear for all applied gate voltages between $-20\,\text{V} < V_g < 20\,\text{V}$.

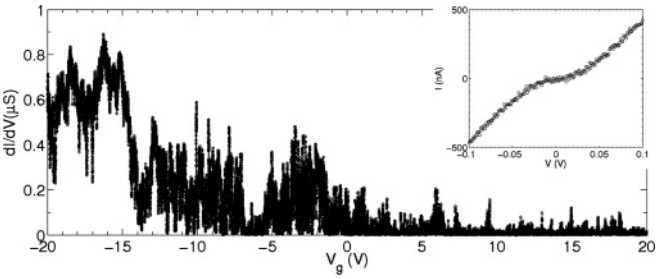

FIG. 5. I-V characteristics (inset, measured at $V_g = 0$ V) and gate voltage response of the individual (17,22) SWCNT measured at 4.3 K. The gate voltage response was measured at zero source drain voltage using standard lock in techniques with an excitation voltage of 400 μV.

The response of the (17,22) top electrode device to an applied gate voltage shows a weak decline in the conductance with positive V_g. This type of behavior has typically been attributed to metallic SWCNTs,[36] and is not what is expected from a semiconducting SWCNT with a band gap of 0.31 eV.

It is known that SWCNTs can be doped by exposure to oxygen[37] and various gaseous species.[38] It is possible that the semiconducting (17,22) SWCNT has been so heavily doped as to appear metallic at room temperature within the applied gate voltage range.

The electronic properties of the device measured at ~4.3 K are shown in Fig. 5. The I-V characteristics are nonlinear with a region of low conductance at small source-drain bias. The differential conductance (dI_{sd}/dV_{sd}) measured as a function of applied gate voltage shows a transition from conducting at large negative V_g to nonconducting with oscillatory conducting peaks for all positive V_g. This behavior is typical of SWCNT devices measured at low temperatures, and can be understood by considering the Schottky barrier formed at the metal-SWCNT interface.[39] For large negative V_g the Schottky barrier is small and the device behaves as an open channel with oscillations due to Fabry-Perot-like interference effects. At positive V_g the Schottky barrier is large and the SWCNT forms a quantum dot with finite conductance only at values of V_g which overcome the charging energy of the dot.

A high resolution bias spectroscopy plot of a region of small positive V_g is shown in Fig. 6. In this particular region of applied V_g Coulomb blockade diamonds with a four-fold periodicity can be seen. The small diamonds (marked 2–4) correspond to the filling of the four-fold degenerate levels

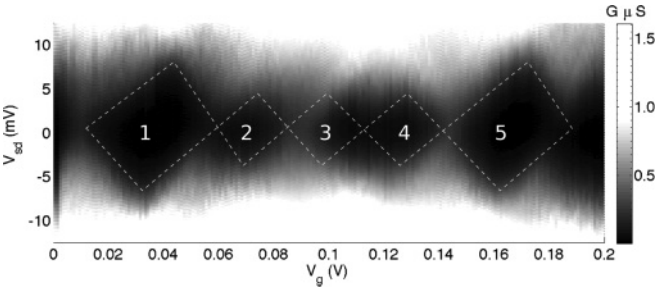

FIG. 6. Differential conductance as a function of V_{sd} and V_g of the individual (17,22) SWCNT measured at 4.3 K using standard lock in techniques with an excitation voltage of 50 μV.

(two spin and two orbital) with the magnitude of the blocked region in V_{sd} being the charging energy of the dot, $\Delta V_{sd} = U_c$ (Ref. 40). The larger diamonds (1 and 5) correspond to the addition of an electron to an empty level and as such the magnitude of the blocked region in V_{sd} is equal to U_c, plus ΔE, the energy level spacing.

For this device in this particular region of applied gate voltage the charging energy is measured to be $U_c \sim 4.8$ meV and the energy level spacing $\Delta E \sim 3.9$ meV. Using the relationship $U_c = \frac{e^2}{C}$ the capacitance of the dot is estimated to be $C \sim 33$ aF (Ref. 41). This can be compared to the expected value using the equation for the capacitance of a coaxial cable,[36]

$$\frac{C}{L} = \frac{2\pi\kappa\epsilon_0}{\ln\left(\frac{2t}{D_0}\right)}, \tag{3}$$

with $\kappa = 2.5$ the average dielectric constant of SiO_2 and air, ϵ_0 the permittivity of free space, $t = 200$ nm the SiO_2 thickness and D_0 the diameter of the SWCNT. As the device length is $L \sim 500$ nm the expected capacitance is $C = 16$ aF, half of the measured value.

Assuming both spin and orbital degeneracy, the energy level spacing can be estimated from[41]

$$\Delta E = \frac{dE}{dk}\Delta k = \hbar v_f \frac{\pi}{L}. \tag{4}$$

Using $v_f = 8.1 \times 10^5$ m/s, the Fermi velocity in graphite[42] the energy level spacing is predicted to be $\Delta E \sim 3.4$ meV, very close to the measured value.

The reasonable agreement of the measured values of U_c and ΔE with estimates suggests that the dot is defined by the portion of the SWCNT which lies in between the electrodes. The lack of regular Coulomb blockade oscillations over a large region of applied V_g is most likely caused by disorder due to defects in the tube, residue from the fabrication process, or substrate roughness.

Irradiation of carbon nanotubes by a low energy electron beam is known to cause a build up of amorphous carbon material.[43] Due to the large ammount of SEM imaging inherent in the fabrication process, it is highly likely that the carbon nanotubes and electodes are contaminated with amorphous carbon material. This contamination could well explain the low device conductance, forming an amorphous carbon barrier between the tube and electrode, and the irregularity of Coulomb blockade oscillations, with a coating of amorphous carbon introducing disorder along the tube.

IV. CONCLUSION AND OUTLOOK

In this work we have described a technique which allows for the fabrication of electronic devices from carbon nanotubes of determined chiral indices. Structural characterization from the analysis of electron diffraction patterns of SWCNTs enabled the confident assignment of chiral indices. The physical transfer of selected tubes from a TEM grid to prepatterned electrodes using STM tips has been demonstrated and good electrical contact achieved. When measured at both room and cryogenic temperatures, completed devices showed electronic behavior typical of SWCNTs.

We hope to build on this work by studying large numbers of characterized SWCNT samples and comparing their transport behavior to that predicted theoretically, and investigating the effects of doping.

Using this technique, not only can the electronic properties of individual SWCNTs be explored, but also ropes containing multiple tubes. This will enable the future study of interactions between the various tubes in a rope.

Furthermore, we envisage studying transport through double and multiwall tubes and hope to use this technique to investigate the effect of encapsulating various species inside SWCNTs on the electronic transport properties.

ACKNOWLEDGMENTS

The authors would like to thank EPSRC for financial support. C.S.A. acknowledges funding from the QIP IRC.

*christopher.allen@materials.ox.ac.uk; Present address: Department of Materials, University of Oxford, Parks Road, Oxford OX1 3PH, United Kingdom.

[1] R. Saito, M. Fujita, G. Dresselhaus, and M. S. Dresselhaus, Appl. Phys. Lett. **60**, 2204 (1992).
[2] A. Kleiner and S. Eggert, Phys. Rev. B **63**, 073408 (2001).
[3] M. Y. Sfelr, T. Beetz, F. Wang, L. Huang, X. M. H. Huang, M. Huang, J. Hone, S. O'Brien, J. A. Misewich, T. F. Heinz, L. Wu, Y. Zhu, and L. E. Brus, Science **312**, 554 (2006).
[4] A. Jorio, R. Saito, J. H. Hafner, C. M. Lieber, M. Hunter, T. McClure, G. Dresselhaus, and M. S. Dresselhaus, Phys. Rev. Lett. **86**, 1118 (2001).
[5] L. Qin, Rep. Prog. Phys. **69**, 2761 (2006).
[6] Y. Sato, K. Yanagi, Y. Miyata, K. Suenaga, H. Kataura, and S. Iijima, Nano Lett. **8**, 3151 (2008).
[7] J. Wildoer, L. Venema, A. Rinzler, R. Smalley, and C. Dekker, Nature (London) **391**, 59 (1998).
[8] S. Iijima and T. Ichihashi, Nature (London) **363**, 603 (1993).
[9] A. Hashimoto, K. Suenaga, A. Gloter, K. Urita, and S. Iijima, Nature (London) **430**, 870 (2004).
[10] S. Piscanec, M. Lazzeri, J. Robertson, A. C. Ferrari, and F. Mauri, Phys. Rev. B **75**, 035427 (2007).
[11] G. Lolli, L. Zhang, L. Balzano, N. Sakulchaicharoen, Y. Tan, and D. E. Resasco, J. Phys. Chem. B **110**, 2108 (2006).
[12] L. Wei, B. Wang, T. H. Goh, L.-J. Li, Y. Yang, M. B. Chan-Park, and Y. Chen, J. Phys. Chem. B **112**, 2771 (2008).
[13] M. S. Arnold, A. A. Green, J. F. Hulvat, S. I. Stupp, and M. C. Hersam, Nat. Nanotechnol. **1**, 60 (2006).
[14] X. Tu, S. Manohar, A. Jagota, and M. Zheng, Nature (London) **460**, 250 (2009).
[15] B. Chandra, R. Caldwell, M. Huang, L. Huang, M. Y. Sfelr, S. P. O'Brien, T. F. Hwinz, and J. Hone, Phys. Status Solidi **243**, 3359 (2006).

[16]L. Y. Jiao, X. J. Xian, Z. Y. Wu, J. Zhang, and Z. F. Liu, Nano Lett. **9**, 205 (2009).
[17]M. Kociak, K. Suenaga, K. Hirahara, Y. Saito, T. Nakahira, and S. Iijima, Phys. Rev. Lett. **89**, 155501 (2002).
[18]T. Kim, G. Kim, W. I. Choi, Y.-K. Kwon, and J.-M. Zuo, Appl. Phys. Lett. **96**, 173107 (2010).
[19]J. Cao, Q. Wang, M. Rolandi, and H. Dai, Phys. Rev. Lett. **93**, 216803 (2004).
[20]C. S. Allen, M. D. Elkin, C. Zhang, S. Hofmann, G. Burnell, J. Robertson, and B. J. Hickey, J. Phys. Conf. Ser. **241**, 012082 (2010).
[21]M. Gao, J. M. Zuo, R. D. Twesten, I. Petrov, L. A. Nagahara, and R. Zhang, Appl. Phys. Lett. **82**, 2703 (2003).
[22]Z. Liu, Q. Zhang, and L.-C. Qin, Appl. Phys. Lett. **86**, 191903 (2005).
[23]L. Qin, Phys. Chem. Chem. Phys. **9**, 31 (2007).
[24]H. Jiang, A. G. Nasibulin, D. P. Brown, and E. I. Kauppinen, Carbon **45**, 662 (2007).
[25]S. Amelinckx, A. Lucas, and P. Lambin, Rep. Prog. Phys. **62**, 1471 (1999).
[26]Z. Liu and L. Qin, Chem. Phys. Lett. **408**, 75 (2005).
[27]H. Jiang, D. P. Brown, A. G. Nasibulin, and E. I. Kauppinen, Phys. Rev. B **74**, 035427 (2006).
[28]C. Qin and L. M. Peng, Phys. Rev. B **65**, 0155431 (2002).
[29]C. S. Allen, C. Zhang, G. Burnell, A. P. Brown, J. Robertson, and B. J. Hickey, Carbon **49**, 4961 (2011).
[30]C. T. White, D. H. Robertson, and J. W. Mintmire, Phys. Rev. B **47**, 5485 (1993).
[31]S. Reich, C. Thomsen, and J. Maultzch, *Carbon Nanotubes Basic Concepts and Physical Properties* (Wiley, New York, 2004).
[32]J. C. Charlier, X. Blase, and S. Roche, Rev. Mod. Phys. **79**, 677 (2007).
[33]A. Kleiner and S. Eggert, Phys. Rev. B **64**, 113402 (2001).
[34]S. Datta, *Electronic Transport in Mesoscopic Systems* (Cambridge University Press, Cambridge, England, 1997), Vol. 1.
[35]R. Saito, G. Dresselhaus, and M. S. Dresselhaus, *Physical Properties of Carbon Nanotubes* (Imperial College Press, London, 1998).
[36]M. J. Biercuk, S. Ilani, C. M. Marcus, and P. L. McEuen, in *Carbon Nanotubes, Advanced Topics in the Synthesis, Structure Properties and Applications*, edited by A. Jorio, M. S. Dresselhaus, and G. Dresselhaus (Springer, New York, 2008), Chap. 15, Electrical Transport in Single-Walled Carbon Nanotubes.
[37]V. Derycke, R. Martel, J. Appenzeller, and P. Avouris, Appl. Phys. Lett. **80**, 2773 (2002).
[38]J. Kong, N. R. Franklin, C. Zhou, M. G. Chapline, S. Peng, K. Cho, and H. Dai, Science **287**, 622 (2000).
[39]T. Kamimura and K. Matsumoto, J. Appl. Phys. **106**, 113718 (2009).
[40]D. H. Cobden and J. Nygard, Phys. Rev. Lett. **89**, 046803 (2002).
[41]J. Nygard, D. Cobden, M. Bockrath, P. McEuen, and P. Lindelof, Appl. Phys. A **69**, 297 (1999).
[42]P. R. Wallace, Phys. Rev. **71**, 622 (1947).
[43]F. Banhart, Nano Lett. **1**, 329 (2001).